2nd Advanced Optical Metrology Compendium

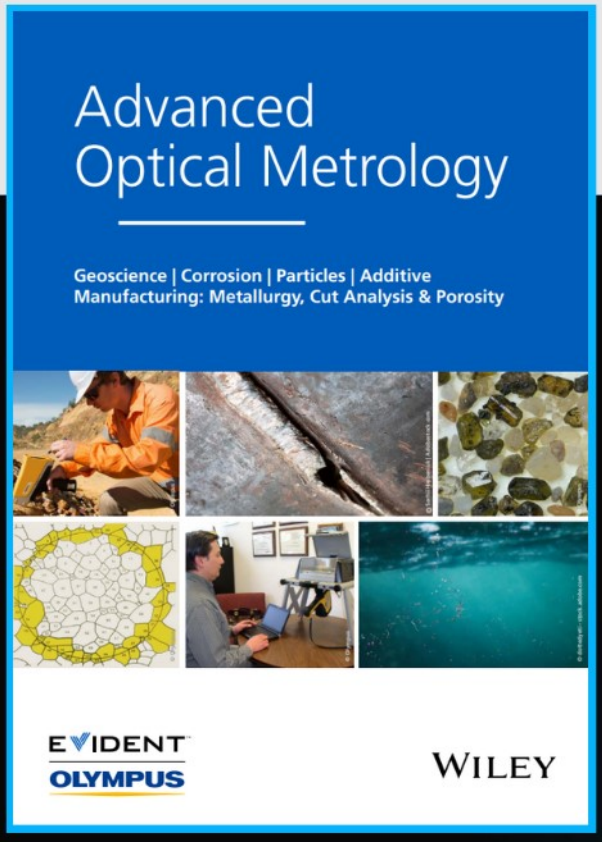

The latest eBook from Advanced Optical Metrology. Download for free.

This compendium includes a collection of optical metrology papers, a repository of teaching materials, and instructions on how to publish scientific achievements.

With the aim of improving communication between fundamental research and industrial applications in the field of optical metrology we have collected and organized existing information and made it more accessible and useful for researchers and practitioners.

EVIDENT
OLYMPUS

WILEY

NANO · MICRO small
www.small-journal.com

Lateral Heterostructures of Graphene and h-BN with Atomic Lattice Coherence and Tunable Rotational Order

Haojie Guo, Ane Garro-Hernandorena, Antonio J. Martínez-Galera,* and José M. Gómez-Rodríguez*

In-plane heterostructures of graphene and hexagonal boron nitride (h-BN) exhibit exceptional properties, which are highly sensitive to the structure of the alternating domains. Nevertheless, achieving accurate control over their structural properties, while keeping a high perfection at the graphene-h-BN boundaries, still remains a challenge. Here, the growth of lateral heterostructures of graphene and h-BN on Rh(110) surfaces is reported. The choice of the 2D material, grown firstly, determines the structural properties of the whole heterostructure layer, allowing to have control over the rotational order of the domains. The atomic-scale observation of the boundaries demonstrates a perfect lateral matching. In-plane heterostructures floating over an oxygen layer have been successfully obtained, enabling to observe intervalley scattering processes in graphene regions. The high tuning capabilities of these heterostructures, along with their good structural quality, even around the boundaries, suggest their usage as test beds for fundamental studies aiming at the development of novel nanomaterials with tailored properties.

1. Introduction

The first experimental isolation of graphene marked the beginning of a new research era, implying the advent of a groundbreaking paradigm for fundamental studies on condensed matter physics.[1] Thus, this carbon sheet of one atom thickness becomes a platform for the experimental demonstration of a large variety of intriguing physical phenomena, not observed previously in any other material.[1–6] It triggered a boom of research, which was rapidly extended to other members of the ever-growing family of 2D materials.[7–11]

Given the extraordinary properties of the different relatives of this family, which is characterized by a high complementarity between its members, the focus of the research was shifted toward their combination into novel nanocomposites with specific properties.[12] For the case of heterostructures, obtained by integration of graphene and hexagonal boron nitride (h-BN) into a single layer composite, interesting tunable electronic,[13,14] thermal conductivity,[15] magnetic,[16–18] and optical[19] properties were reported. However, the precise tuning of these properties relies on the control of parameters as size, shape, atomic-scale structure of the domains of both materials, and perfection of the lattice-matching at the boundaries.

In order to be able to achieve a controlled tune of the properties of the lateral heterostructures, as well as to induce in them novel functionalities, it is mandatory the development of model systems that allows to selectively vary the above-mentioned structural parameters. Notwithstanding, in some cases, graphene and h-BN regions adopt, respectively, the same in-plane lattice orientations with respect to the metal surface as they are present in the absence of the other 2D material.[20–23] Hence, these systems do not offer the possibility of tunning the rotational order within the heterostructure layer. In contrast, in systems characterized by a weaker interaction of both 2D materials with the support, it was found that one of the 2D materials adopts the lattice orientations of the other.[24–26] However, the possibility of systematically setting the rotational order in a given heterostructure/metal system, by inverting the growth sequence of both 2D materials, has not been demonstrated yet. It should be noted that being able to set

H. Guo, A. Garro-Hernandorena, J. M. Gómez-Rodríguez
Departamento de Física de la Materia Condensada
Universidad Autónoma de Madrid
Madrid E-28049, Spain
E-mail: haojie.guo@uam.es

A. J. Martínez-Galera
Departamento de Física de Materiales
Universidad Autónoma de Madrid
Madrid E-28049, Spain
E-mail: antonio.galera@uam.es

A. J. Martínez-Galera, J. M. Gómez-Rodríguez
Instituto Nicolás Cabrera
Universidad Autónoma de Madrid
Madrid E-28049, Spain

J. M. Gómez-Rodríguez
Condensed Matter Physics Center (IFIMAC)
Universidad Autónoma de Madrid
Madrid E-28049, Spain

The ORCID identification number(s) for the author(s) of this article can be found under https://doi.org/10.1002/smll.202207217.

The first published online date is 7th January 2023.

DOI: 10.1002/smll.202207217

the lattice orientations of graphene and h-BN, implies setting the moiré superstructures, which rule the interfacial physical and chemical properties. Besides rotational order, the lateral epitaxy to accommodate the atomic lattices of both 2D materials is also of paramount importance, given the influence of the boundaries in most of the properties of graphene and h-BN lateral heterostructures, although, to date, it remains almost unexplored by direct visualization at the atomic scale. Only a few theoretical and experimental works have tackled these issues from a microscopic and atomistic point of view.[27,28] In these works, it has been shown how sharp and straight interfaces between graphene and h-BN can be obtained through the control of carbon concentration and h-BN coverage, as well as through their interaction with the metal support. Accordingly, the influence of the rotational order on the lateral epitaxy also needs to be investigated, since it could provide a pathway for further tuning of the properties of heterostructures.

In this work, the growth and atomic-scale visualization of in-plane heterostructures of one atomic level, with high structural quality, comprising single-layer graphene and h-BN flakes on Rh(110) surfaces is reported. It is demonstrated that, for these nanomaterials, configurational parameters as the rotational order can be easily tuned. Remarkably, the graphene-h-BN boundaries are found to be atomically sharp, displaying a perfect lateral epitaxy. As a last step to enlarge their potential, efficient decoupling of these in-plane heterostructures from the metal substrate has been achieved by oxygen intercalation. Because of all of it, they have all the ingredients to be used as testbeds for fundamental studies, oriented toward achieving a controlled tune of the properties of graphene and h-BN lateral heterostructures through accurate control of key structural parameters.

2. Results and Discussion

Two different kinds of lateral heterostructures have been grown, which will hereinafter be denoted as G_h-BN and h-BN_G. Both were obtained through a two steps process, being the main difference the growth sequence of graphene and h-BN. The first step consisted of the room temperature (RT) exposure of the Rh(110) surface to the precursor (ethylene for G_h-BN heterostructures, or borazine for h-BN_G ones), and subsequent annealing. The second step consisted of a chemical vapor deposition (CVD) process, using borazine as a precursor for G_h-BN heterostructures and ethylene for h-BN_G ones. See the experimental section for further details.

As mentioned in the previous paragraph, the procedure developed in this work to obtain the G_h-BN heterostructures consists of two steps. In order to achieve a better understanding of the whole approach, **Figure 1** collects the most relevant features of the samples after the first growth step. Specifically, a representative low energy electron diffraction (LEED) pattern of this growth stage is shown in Figure 1a. It displays, along with the atomic periodicity of the Rh(110) surface, the characteristic arcs of graphene, associated with the coexistence of multiple rotational domains, which is consistent with a previous work on full layer graphene grown on Rh(110).[29] Sample morphology, as revealed by large scale scanning tunneling microscope (STM) images (see Figure 1b), is characterized by graphene islands grown on the Rh(110) support, covering ≈30% of its surface. High resolution STM images acquired inside the islands (see Figure 1c,d) show, along with the atomic periodicity of graphene, stripe-like moiré patterns akin to the ones previously reported for graphene monolayers grown on Rh(110).[29]

Once the effects of the first growth step have been addressed, the analysis of the morphological and structural features of the G_h-BN in-plane heterostructures, obtained after a subsequent CVD process using borazine as a precursor, will be presented. **Figure 2**a shows a typical LEED pattern obtained in these samples, which displays the characteristic arcs of graphene grown on this metal surface (compare with Figure 1a). From the point of view of sample morphology, STM images as that shown in Figure 2b prove that the surface is dominated by the coexistence of regions with differently oriented moiré stripes. Interestingly, domains with apparent heights differing from the rest of the surface (see also Figure S1, Supporting Information), are found scattered over the sample. It suggests the coexistence of two different materials, which tentatively could be ascribed to the success of growing the G_h-BN lateral heterostructures. On the basis of this argument, a direct comparison with the typical graphene coverages reached after the first growth step (Figure 1b) would suggest that the closed domains could be graphene flakes. However, surprisingly, STM images as those shown in Figure 2c,d prove that both the moiré stripes and the atomic arrangement are equally oriented at both sides of the boundary. Moreover, the atomic periodicities characteristic of the two equivalent rotational domains of h-BN over Rh(110), previously characterized in a recent work,[30] is not present in LEED patterns as that exhibited in Figure 2a, although B and N are detected in Auger electron spectroscopy (AES) measurements (see Figure S2, Supporting Information). Then, all this together suggests that h-BN grows based on the graphene arrangement, giving rise to a lateral heterostructure. Here it is convenient to remind that the difference between lattice parameters of pristine graphene and h-BN is below 2%.

Now, the approach employed to obtain the in-plane h-BN_G heterostructures will be analyzed. **Figure 3** summarizes the main morphological and structural features of the samples resulting from the first growth step: exposure of the Rh(110) surface at RT to borazine, and annealing in the experimental conditions described in the methods section. In particular, a representative LEED pattern of the so obtained samples is presented in Figure 3a. It shows the rectangular lattice of Rh(110), along with two intense sets of spots (highlighted by blue and red circumferences), revealing the existence of two rotational variants with specular symmetry, which, hence, are isostructural. It is in agreement with the previously reported LEED analysis of h-BN monolayers grown on Rh(110) surfaces.[30] Sample morphology, as revealed by STM images as that shown in Figure 3b,c, is dominated by the existence of h-BN covering around 60% of the Rh(110) surface. According to the existence of the two isostructural domains, high resolution STM images show a periodic pattern, consisting of quasi-1D fringes separated by 1.4 nm, exhibiting a twist angle of ~ 20 with respect to the atomic arrangement (see Figure 3d), which are found along the sample with two possible orientations: It is in agreement

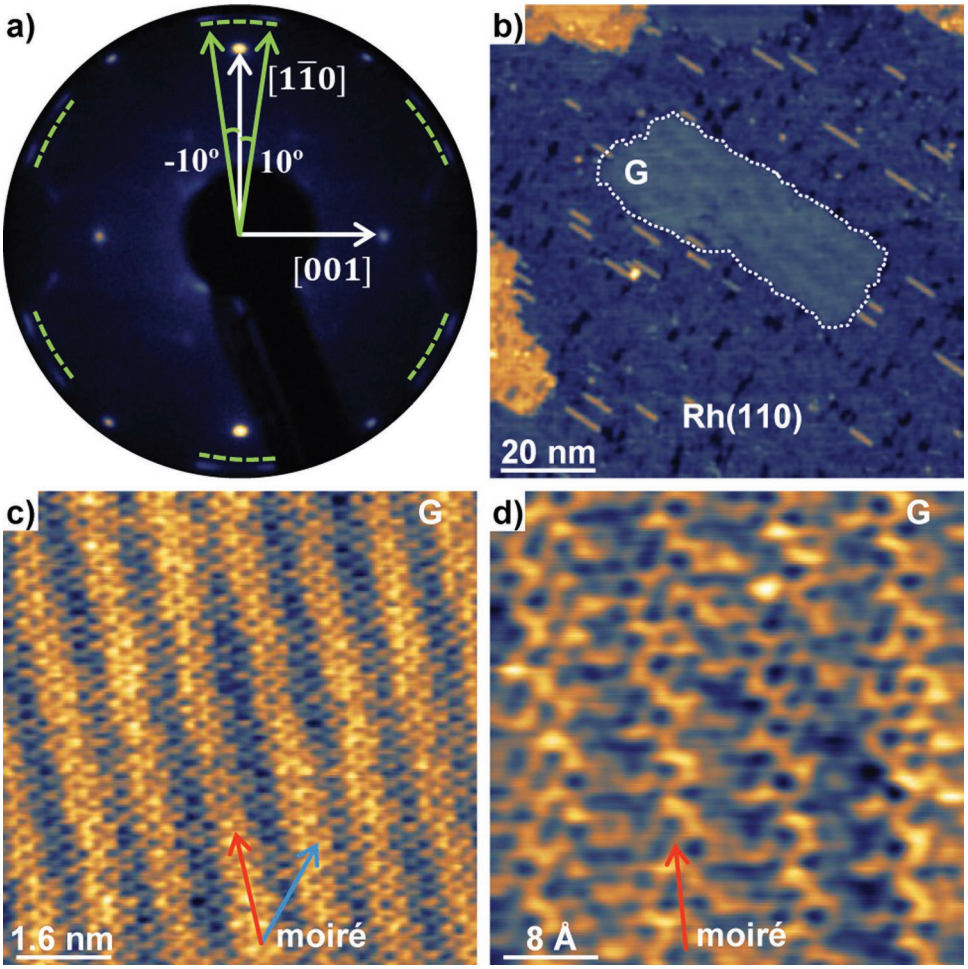

Figure 1. Structural characterization of G/Rh(110) obtained after the first growth step of G_h-BN heterostructures. a) LEED pattern acquired with an electron energy of E = 72 eV. b) STM image of the as grown surface, where a graphene flake, highlighted in white, can be observed along with bare Rh(110). c) STM image with atomic resolution on a graphene flake. The red and blue arrows indicate the direction of each of the two sets of fringes that compose the moiré superstructure observed in this sample region. d) Atomically resolved STM image on a flake of graphene on Rh(110). The moiré direction is indicated by the arrow. Tunneling parameters: b) $V_s = 2$ V; $I_t = 0.8$ nA; size: 100×100 nm^2. c) $V_s = 15$ mV; $I_t = 19.2$ nA; size: 8×8 nm^2. d) $V_s = 20$ mV; $I_t = 18.7$ nA; size: 4×4 nm^2.

with previous studies performed on full h-BN monolayers grown on Rh(110) surfaces.[30]

Figure 4 summarizes the study performed after the second growth step of the h-BN_G heterostructures, consisting of a CVD process, using ethylene as a precursor. Figure 4a presents a typical LEED pattern, acquired at this stage, which is identical to those acquired in the previous step (compare with Figure 3a). Consistent with the existence of two sets of spots in LEED patterns, STM images as that shown in Figure 4b exhibit a surface comprising domains with only two orientations of the moiré fringes. For some of these regions, the apparent height differs from the rest of the sample. A typical atomic resolution STM image around the boundary between domains of both kinds with contrasting apparent heights is provided in Figure 4c. As observed, the atomic arrangements of both regions are aligned with respect to each other.

The similarities between the LEED patterns shown in Figure 3a and 4a, demonstrating the absence of the characteristic arcs of graphene on Rh(110), along with STM images as that shown in Figure 4b, which displays the existence of uniquely two specular domains instead of multiple orientations, seem to indicate the absence of graphene after the second growth step. Nevertheless, AES measurements show the existence of carbon in the sample (see Figure S3). This fact, along with the presence of regions with contrasting apparent heights, leads to the conclusion that graphene regions are coexisting with h-BN ones over the Rh(110) surface. Thus, according to STM images as that shown in Figure 4b, it can be inferred that the kind of regions covering a smaller fraction of the metal surface is graphene islands. However, the in-plane orientations of the atomic arrangements of these graphene domains over the Rh(110) surface differ from these, observed in Figure 1, for graphene islands grown on that metal support in the absence of the h-BN flakes. Actually, the in-plane orientations of the atomic arrangements along the whole layer resemble these of the initially grown h-BN flakes (see Figure 3). Therefore, it is concluded that the arrangement of C atoms during graphene growth is templated by the structure of the h-BN domains,

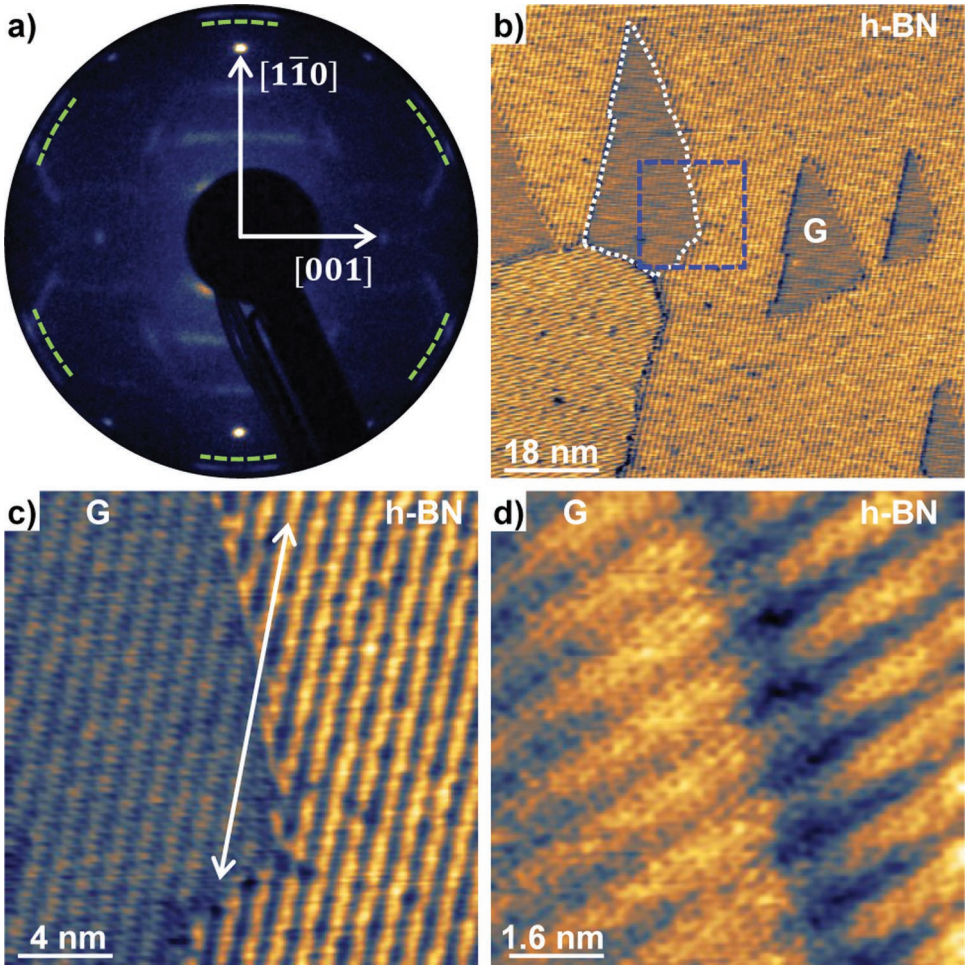

Figure 2. Structural characterization of G_h-BN lateral heterostructures grown on Rh(110). a) LEED pattern acquired with an electron energy of 72 eV on a G_h-BN/Rh(110) surface. b) STM image of G_h-BN showing domains with two different directions of the moiré superstructure. Besides, regions, like the one highlighted in white, with dissimilar apparent heights demonstrate the coexistence of two different materials on the surfaces. c) Zoom-in STM image within the dotted blue square indicated in (b). The white line manifests that the stripe-like moiré structures have the same orientation at both sides of the boundary between the two materials. d) Atomically resolved STM image showing the alignment of both, the moiré fringes and the atomic arrangements, across the boundary. Tunneling parameters: b) $V_s = 0.25$ V; $I_t = 4.2$ nA; size: 90×90 nm^2. c) $V_s = 0.25$ V; $I_t = 4.2$ nA; size: 20×20 nm^2. d) $V_s = 5$ mV; $I_t = 21.1$ nA; size: 8×8 nm^2.

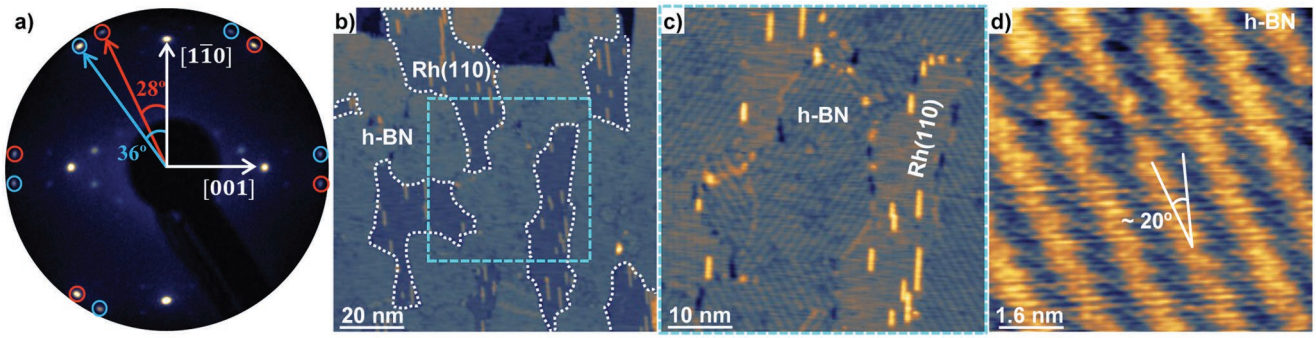

Figure 3. Structural characterization of h-BN/Rh(110) obtained after the first growth step of h-BN_G heterostructures. a) LEED pattern acquired at an electron energy of 72 eV. b) STM image of h-BN/Rh(110) showing bare Rh(110) areas, which are enclosed by white dotted lines. c) STM image acquired in the square region highlighted in (b), where two moiré directions are visible. d) STM image with atomic resolution on an h-BN flake. Tunneling parameters: b) $V_s = 2$ V; $I_t = 1$ nA; size: 100×100 nm^2. c) $V_s = 0.48$ V; $I_t = 2.4$ nA; size: 50×50 nm^2. d) $V_s = 20$ mV; $I_t = 14.8$ nA; size: 8×8 nm^2.

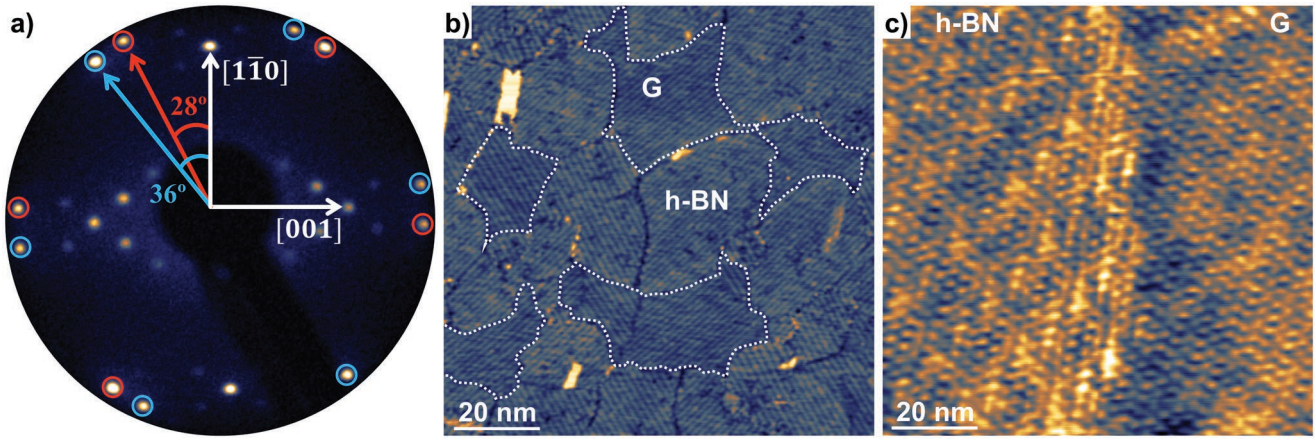

Figure 4. Structural characterization of h-BN_G/Rh(110) heterostructures. a) LEED pattern of a h-BN_G sample obtained at an electron energy of 72 eV. b) STM image acquired on a h-BN_G lateral heterostructure sample. Graphene islands are enclosed by white dotted lines to guide the eye. All flakes exhibit uniquely two possible rotational domains. c) STM image with atomic resolution around a boundary between a graphene region and a h-BN one. Tunneling parameters: b) $V_s = 1.8$ V; $I_t = 1$ nA; size: 90×90 nm^2. c) $V_s = -12$ mV; $I_t = 19.2$ nA; size: 8×8 nm^2.

initially grown during the first growth step. Further support for that statement is found in Figure 4c, where the same atomic orientation at both sides of the boundary between regions exhibiting different apparent heights is observed.

In definitive, for both kinds of lateral heterostructures, the atomic arrangement of the firstly grown 2D material is the one that defines the structure of the entire sample, after the growth step of the other component. It is at variance with previous studies reporting the growth of graphene and h-BN in-plane heterostructures on Rh(111),[21] Ru(0001),[20] Ni(111),[23] and Ir(111),[22] where graphene and h-BN regions exhibit the same atomic arrangements over the metal surface as they present in the absence of the other 2D material. In other words, on these metal surfaces, the interaction of both graphene and h-BN with the metal support seems to be more decisive than that at the boundaries between both 2D materials. In contrast, on Cu foils, it was reported that, due to the weaker interaction of both 2D materials with the support, h-BN adopts the orientation of the initially grown graphene flakes instead of that energetically favored one in the absence of the latter.[24,25] Conversely, graphene was found to be aligned to the initially grown h-BN islands, instead of adopting the multiple lattice orientations characteristic of the G/Pt(111) interface.[26] Therefore, the experimental findings presented here for the graphene and h-BN in-plane heterostructures, grown on Rh(110), are more similar to those reported on Pt(111) and Cu foils. It suggests that the interaction strength of graphene and h-BN with the Rh(110) support could be comparable to that between these 2D materials and the surfaces of Pt(111) and Cu. However, the work presented here demonstrates the alignment between both materials, for the two possible growth sequences, in such a way that, depending on whether either graphene or h-BN is grown firstly, the possible orientations of the resulting heterostructures with respect to the underlying Rh(110) surface are different in each case. Therefore, the choice of the growth sequence allows setting the rotational order along the lateral heterostructure. In particular, this rotational order is characterized by the existence of only two specular domains if h-BN is grown first, while by inverting the growth sequence, the whole heterostructure sample is dominated by the coexistence of domains with infinite orientations. Accordingly, given that the 2D material-substrate interfacial interaction is in general different for each rotational domain, it allows setting the electronic and chemical properties of the graphene and h-BN flakes comprising the heterostructure. Regarding the atomic-scale configuration of the graphene-h-BN interfaces, a deeper inspection of STM images as those displayed in Figure 2d and Figure 4c, suggests that the boundaries are mostly parallel to the atomic lattices of both materials. It is a signature of a preference for a linking interface dominated by zigzag edges, regardless of the growth sequence. Likewise, the perfect linking of the lattices of both materials is translated into a perfect matching also of the moiré pattern across the boundaries. Furthermore, it is interesting to note that the differences between the in-plane graphene and h-BN heterostructures grown, in this work, on Rh(110), and their counterparts, previously reported on Rh(111), provide a demonstration that the structural properties of the lateral heterostructures of these 2D materials strongly depend on the crystallography of the supporting surface.

Once the growth of the lateral heterostructures was achieved, and a systematic control of their structural properties was reached, the research described here intended to go one step further away, aiming to obtain graphene and h-BN heterostructures as much uncoupled as possible from the metal support. The methodology employed consisted of the intercalation of oxygen between the heterostructure layer and the Rh(110) surface. **Figure 5**a shows a typical LEED pattern acquired after exposure to O_2, in the way described in the methods section, a previously grown G_h-BN sample. The set of six angularly equispaced arcs characteristic of G/Rh(110) (see Figure 1a) and of G_h-BN samples (see Figure 2a) is observed. Accordingly, Figure 5c shows a typical LEED pattern obtained for a h-BN_G sample, after oxygen exposure at identical experimental conditions. It shows the two sets of spots, characteristic of h-BN/Rh(110) (Figure 3a), which are also observed in as-grown h-BN_G samples (Figure 4a). Nevertheless, the corresponding LEED patterns obtained before O_2 exposure (Figure 2a and 4a), display different sets of spots associated with the periodicity of the moiré stripes, which are

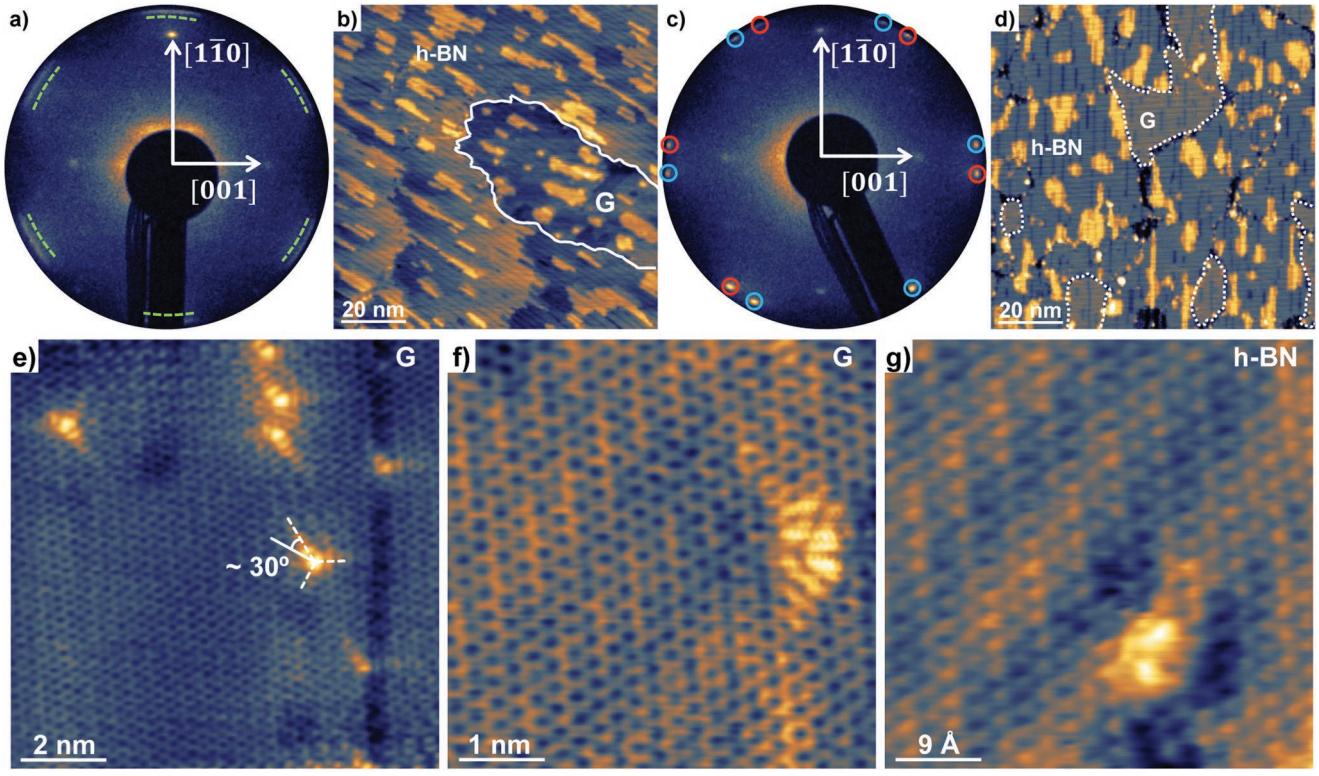

Figure 5. Structural characterization of G_h-BN and h-BN_G samples after O intercalation by O_2 exposure. a) Typical LEED pattern of a G_h-BN/O/Rh(110) sample (E = 72 eV). b) STM image of G_h-BN/O/Rh(110). Graphene areas are enclosed by white dotted lines to guide the eye. c) Typical LEED pattern of a h-BN_G/O/Rh(110) sample (E = 72 eV). d) STM image of h-BN_G/O/Rh(110). e) STM image with atomic resolution on a graphene flake, displaying intervalley scattering processes around point defects. f) STM image with atomic resolution on a graphene flake, showing a close view of a point defect giving rise to intervalley scattering. g) STM image with atomic resolution on a h-BN domain with a point defect, showing no intervalley scattering features. Tunneling parameters: b) V_s = 0.5 V; I_t = 1 nA; size: 100 × 100 nm^2. d) V_s = 2 V; I_t = 1.5 nA; size: 100 × 100 nm^2. e) V_s = 0.2 V; I_t = 2.9 nA; size: 9 × 9 nm^2. f) V_s = 40 mV; I_t = 14.4 nA; size: 5 × 5 nm^2. g) V_s = 30 mV; I_t = 8.1 nA; size: 4.5 × 4.5 nm^2.

no longer present in the respective LEED patterns (Figure 5a,c) acquired after oxygen exposure. Consistently, the moiré stripes become only faintly observed in STM images acquired on both G_h-BN and h-BN_G samples after O_2 exposure as described in the experimental section (see Figure 5f,g).

Similar effects—the absence, in LEED patterns, of spots associated with moiré superstructures, and the significant decrease in the apparent corrugation of the moiré stripes in STM images—have been previously reported after oxygen intercalation between a graphene layer and metal support.[31,32] Then, it can be concluded that a layer of oxygen is intercalated at the interface of the graphene and h-BN heterostructures with the Rh(110) support.

Further evidence of O intercalation is found in rows as that observed along the vertical direction of the STM image shown in Figure 5e and in Figure S4 (Supporting Information). They resemble the missing rows reconstructions observed after the dissociative chemisorption of O_2 on Rh(110).[33] Interestingly, the atomic periodicity with hexagonal symmetry characteristic of both 2D materials comprising the heterostructure, which differs from the rectangular one of the Rh(110) surface, is observed even over the rows (see Figure 5e). It means that these rows must be associated with atomic arrangements below the 2D material. Then, the presence of these rows also points toward a scenario, in which the lateral graphene and h-BN heterostructures are resting on an intercalated O layer chemisorbed to the underlying Rh(110) surface.

As a result of O intercalation, STM images as those shown in Figure 5b,d exhibit a rather complex sample morphology. Regions displaying a marked contrast of apparent heights can be identified as, either graphene or h-BN (see labeling of Figure 5b,d), according to their relative abundance in the respective as-grown G_h-BN and h-BN_G samples, prior to oxygen exposure.

Additional information about the properties of the lateral heterostructures after O intercalation has been obtained through the study of naturally occurring point defects. The observed features in atomically resolved STM images, as those in Figure 5e,f, around point defects in graphene regions, show the ($\sqrt{3}$ × $\sqrt{3}$)-R30° modulation of the local density of states, associated with intervalley scattering processes of Dirac quasiparticles, characteristic of graphene layers isolated from their local environment.[34–36] Thus, it demonstrates that the oxygen intercalated layer provides an effective decoupling of the heterostructure layer from the Rh(110) support. It is noteworthy to mention that these Dirac quasiparticles scattering processes have not been previously reported on lateral graphene and h-BN heterostructures. On the other hand, point defects in h-BN regions are observed as featureless protrusions (see Figure 5g), regardless of the bias voltage applied to the sample. It could be

explained in terms of the insulating character of h-BN, which implies the absence of free quasiparticles in a wide energy window around the Fermi level.

3. Conclusions

In conclusion, the growth of in-plane lateral structures of graphene and h-BN is reported. The 2D material grown in the first step fixes the atomic arrangement of the whole heterostructure. It allows setting the rotational order of the heterostructure, as well as its interaction with the underlying metal surface by choosing the growth sequence. The linking interface between graphene and h-BN domains is characterized by a perfect lateral epitaxy. These heterostructures have been effectively uncoupled from the Rh(110) support by oxygen intercalation. It has allowed providing the first images displaying Dirac quasiparticle scattering processes in the graphene regions of a lateral heterostructure. The high degree of tuning of these lateral heterostructures and their great structural quality, even around the domain boundaries, confer this system a tremendous potential to be used as a test bed for fundamental research, oriented to obtain novel nanomaterials with tailored properties, based on graphene and h-BN.

4. Experimental section

Experiments were performed in a homemade ultra-high vacuum system, composed of a chamber for sample preparation, and another one for its atomic-scale characterization by means of a home built variable temperature scanning tunneling microscope.[37,38] The former was equipped with state-of-the-art facilities for sample preparation, as well as with an optics for LEED and AES analysis of the sample.

The Rh(110) single crystal was cleaned up, firstly, by Ar^+ sputtering, with an energy of the incident ions of 2 kV, at a sample temperature of 850 °C. Subsequently, the Rh(110) crystal was annealed at 850 °C, firstly in an oxygen atmosphere with a partial pressure of 2×10^{-6} Torr to remove C impurities from the surface and the subsurface, and then without supplying oxygen for 5 min. The cleaning of the metal substrate was concluded with a flash annealing at 1060 °C to ensure O removal.

For G_h-BN heterostructures, in the first step, graphene was grown by exposing the Rh(110) substrate at RT to 36 L of ethylene (C_2H_4), at a partial pressure of this precursor of 3×10^{-7} Torr and subsequent annealing at 800 °C for 1 min. This procedure was cyclically repeated three times. The result was the growth of scattered graphene islands over the Rh(110) surface. In the second step, h-BN was grown by CVD. Specifically, the sample was kept at 800 °C and exposed to 45 L of borazine at 2.5×10^{-8} Torr. This preparation methodology provides a one atom thick layer consisting of graphene flakes randomly distributed into a percolated h-BN layer. For the growth of h-BN_G heterostructures, the first step consisted of exposing the freshly prepared Rh(110) surface at RT to 36 L of borazine at 3×10^{-7} Torr, followed with an annealing step at 820 °C for 5 min, giving rise to h-BN islands randomly scattered over the metal surface. In the second step, graphene was grown by CVD with ethylene (45 L at a partial pressure of 2.5×10^{-8} Torr) with the sample at 800 °C.

Oxygen intercalation, in between the graphene-h-BN monolayer and the Rh(110) surface, was performed, for both kinds of heterostructures by O_2 exposure at a partial pressure of 2×10^{-6} Torr for 75 min, with the sample kept at around 280 °C. It provided lateral G_h-BN and h-BN_G heterostructures floating over an oxygen layer.

STM measurements were performed in the constant current mode, with an electrochemically etched tungsten tip, at RT. The bias voltage was applied to the sample, while the STM tip was grounded. Both data acquisition and analysis were carried out by using the WSxM software.[39]

Supporting Information

Supporting Information is available from the Wiley Online Library or from the author.

Acknowledgements

Antonio J. Martínez-Galera, José M. Gómez-Rodríguez: Deceased. The authors dedicated this work in memory of Prof. José María Gómez Rodríguez, personal friend, mentor, and colleague. Financial support from the Spanish Ministerio de Economía y Competitividad (MINECO) and Fondo Europeo de Desarrollo Regional (FEDER) under grant No. MAT2016-77852-C2-2-R, as well as, from the Spanish Ministerio de Ciencia e Innovación through the "María de Maetzu" program for units of excellence in R&D (grant No. CEX2018-000805-M) was gratefully acknowledged. A. J. M.-G. acknowledged funding by the Spanish Ministerio de Ciencia e Innovación (MICINN through Project No. PID2020-116619GA-C22, as well as, by the Comunidad de Madrid and Universidad Autónoma de Madrid under Project No. SI3/PJI/2021-00500. Funding sources: Spanish MINECO (Ref: MAT2016-77852-C2-2-R). Spanish MICINN (Ref: PID2020-116619GA-C22). Comunidad de Madrid (CAM) and Universidad Autónoma de Madrid (UAM) (Ref: SI3/PJI/2021-00500)

Conflict of Interest

The authors declare no conflict of interest.

Author Contributions

The manuscript was written through contributions of all authors. All authors have given approval to the final version of the manuscript.

Data Availability Statement

The data that support the findings of this study are available from the corresponding author upon reasonable request.

Keywords

2D materials, domain boundaries, lateral heterostructures, oxygen intercalation, scanning tunneling microscope (STM)

Received: November 20, 2022
Revised: January 4, 2023
Published online:

[1] K. S. Novoselov, A. K. Geim, S. V. Morozov, D. Jiang, Y. Zhang, S. V. Dubonos, I. V. Grigorieva, A. A. Firsov, *Science* **2004**, *306*, 666.
[2] K. S. Novoselov, A. K. Geim, S. V. Morozov, D. Jiang, M. I. Katsnelson, I. V. Grigorieva, S. V. Dubonos, A. A. Firsov, *Nature* **2005**, *438*, 197.
[3] Y. B. Zhang, Y.-W. Tan, H. L. Stormer, P. Kim, *Nature* **2005**, *438*, 201.

[4] M. I. Katsnelson, K. S. Novoselov, A. K. Geim, *Nat. Phys.* **2006**, *2*, 620.
[5] K. S. Novoselov, E. McCann, S. V. Morozov, V. I. Fal'ko, M. I. Katsnelson, U. Zeitler, D. Jiang, F. Schedin, A. K. Geim, *Nat. Phys.* **2006**, *2*, 177.
[6] Y. Cao, V. Fatemi, S. Fang, K. Watanabe, T. Taniguchi, E. Kaxiras, P. Jarillo-Herrero, *Nature* **2018**, *556*, 43.
[7] P. Vogt, P. De Padova, C. Quaresima, J. Avila, E. Frantzeskakis, M. C. Asensio, A. Resta, B. Ealet, G. L. Lay, *Phys. Rev. Lett.* **2012**, *108*, 155501.
[8] Q. H. Wang, K. Kalantar-Zadeh, A. Kis, J. N. Coleman, M. S. Strano, *Nat. Nanotechnol.* **2012**, *7*, 699.
[9] A. J. Mannix, X. F. Zhou, B. Kiraly, J. D. Wood, D. Alducin, B. D. Myers, X. L. Liu, B. L. Fisher, U. Santiago, J. R. Guest, M. J. Yacaman, A. Ponce, A. R. Oganov, M. C. Hersam, N. P. Guisinger, *Science* **2015**, *350*, 1513.
[10] F. F. Zhu, W. Chen, Y. Xu, C. Gao, D. Guan, C. Liu, D. Qian, S.-C. Zhang, J. Jia, *Nat. Mater.* **2015**, *14*, 1020.
[11] F. Reis, G. Li, L. Dudy, M. Bauernfeind, S. Glass, W. Hanke, R. Thomale, J. Schafer, R. Claessen, *Science* **2017**, *357*, 287.
[12] J. Wang, Z. Li, H. Chen, G. Deng, X. Niu, *Nano-Micro Lett.* **2019**, *11*, 48.
[13] X. Fan, Z. Shen, A. Q. Liu, J.-L. Kuo, *Nanoscale* **2012**, *4*, 2157.
[14] J. Wang, R. Zhao, Z. Liu, Z. Liu, *Small* **2013**, *9*, 1373.
[15] A. Kinaci, J. B. Haskins, C. Sevik, T. Cagin, *Phys. Rev. B* **2012**, *86*, 115410.
[16] Y. Liu, S. Bhowmick, B. I. Yakobson, *Nano Lett.* **2011**, *11*, 3113.
[17] R. Drost, A. Uppstu, F. Schulz, S. K. Hamalainen, M. Ervasti, A. Harju, P. Liljeroth, *Nano Lett.* **2014**, *14*, 5128.
[18] H. S. Wang, L. Chen, K. Elibol, L. He, H. Wang, C. Chen, C. Jiang, C. Li, T. Wu, C. X. Cong, T. J. Pennycook, G. Argentero, D. Zhang, K. Watanabe, T. Taniguchi, W. Wei, Q. Yuan, J. C. Meyer, X. Xie, *Nat. Mater.* **2021**, *20*, 202.
[19] G. Kim, K. Yeol, M. Park, M. Kim, J. Jeon, J. Song, J. E. Barrios-Vargas, Y. Sato, Y.-C. Lin, K. Suenaga, S. Roche, S. Yoo, B.-H. Sohn, S. Jeon, H. S. Shin, *Nat. Commun.* **2020**, *11*, 5359.
[20] P. Sutter, R. Cortes, J. Lahiri, E. Sutter, *Nano Lett.* **2012**, *12*, 4869.
[21] Y. Gao, Y. Zhang, P. Chen, Y. Li, M. Liu, T. Gao, D. Ma, Y. Chen, Z. Cheng, X. Qju, W. Duan, Z. Liu, *Nano Lett.* **2013**, *13*, 3439.
[22] M. Liu, Y. Li, P. Chen, J. Sun, D. Ma, Q. Li, T. Gao, Y. Gao, Z. Cheng, X. Qiu, Y. Fang, Y. Zhang, Z. Liu, *Nano Lett.* **2014**, *14*, 6342.
[23] W. Wei, J. Pan, C. Euaruksakul, Y. Yang, Y. Cui, Q. Fu, X. Bao, *Nano Res.* **2020**, *13*, 1789.
[24] L. Liu, J. Park, D. A. Siegel, K. F. McCarty, K. W. Clark, W. Deng, L. Basile, J. C. Idrobo, A.-P. Li, G. Gu, *Science* **2014**, *343*, 163.
[25] D. Geng, J. Dong, L. K. Ang, F. Ding, H. Y. Yang, *NPG Asia Mater.* **2019**, *11*, 56.
[26] J. Pan, W. Wei, Z. Gong, Y. Cui, *Carbon* **2021**, *177*, 19.
[27] N. Han, H. Liu, J. Zhang, J. Gao, J. Zhao, *Nanoscale* **2017**, *9*, 3585.
[28] T. H. Nguyen, D. Perilli, M. Cattelan, H. Liu, F. Sedona, N. A. Fox, C. Di Valentin, S. Agnoli, *Nano Res.* **2019**, *12*, 675.
[29] A. J. Martínez-Galera, H. Guo, M. D. Jiménez-Sanchez, E. G. Michel, J. M. Gomez-Rodriguez, Carbon (In Press) **2023**, https://doi.org/10.1016/j.carbon.2023.01.004.
[30] A. J. Martinez-Galera, J. M. Gomez-Rodriguez, *Nano Res.* **2018**, *11*, 4643.
[31] E. Granas, J. Knudsen, U. A. Schroder, T. Gerber, C. Busse, M. A. Arman, K. Schulte, J. N. Andersen, T. Michely, *ACS Nano* **2012**, *6*, 9951.
[32] A. J. Martinez-Galera, U. A. Schroder, F. Huttmann, W. Jolie, F. Craes, C. Busse, V. Caciuc, N. Atodiresei, S. Blugel, T. Michely, *Nanoscale* **2016**, *8*, 1932.
[33] C. Africh, G. Comelli, *J Phys Condens Matter* **2006**, *18*, R387.
[34] G. M. Rutter, J. N. Crain, N. P. Guisinger, T. Li, P. N. First, J. A. Stroscio, *Science* **2007**, *317*, 219.
[35] I. Brihuega, P. Mallet, C. Bena, S. Bose, C. Michaelis, L. Vitali, F. Varchon, L. Magaud, K. Kern, J. Y. Veuillen, *Phys. Rev. Lett.* **2008**, *101*, 206802.
[36] M. M. Ugeda, I. Brihuega, F. Guinea, J. M. Gomez-Rodriguez, *Phys. Rev. Lett.* **2010**, *104*, 096804.
[37] O. Custance, S. Brochard, I. Brihuega, E. Artacho, J. M. Soler, A. M. Baro, J. M. Gomez-Rodriguez, *Phys. Rev. B* **2003**, *67*, 235410.
[38] A. J. Martinez-Galera, J. M. Gomez-Rodriguez, *J. Phys. Chem. C* **2011**, *115*, 11089.
[39] I. Horcas, R. Fernandez, J. M. Gomez-Rodriguez, J. Colchero, J. Gomez-Herrero, A. M. Baro, *Rev. Sci. Instrum.* **2007**, *78*, 013705.